Quantification of Thruster Forces for Escorting Tugs

R.P.M. Schillings

Technische Universiteit Delft

TU Delft

DAMEN

Quantification of Thruster Forces for Escorting Tugs

by

R.P.M. Schillings

to obtain the degree of Master of Science
at the Delft University of Technology,
to be defended publicly on Tuesday July 10, 2018 at 9:30 AM.

Student number:	4174372	
Project duration:	September 4, 2017 – July 10, 2018	
Thesis committee:	Prof. dr. ir. A. P. van 't Veer,	TU Delft, chair
	Dr. ir. P. R. Wellens,	TU Delft, daily supervisor
	Dr. ir. A. Vrijdag,	TU Delft
	Ing. J. de Jong,	Damen Shipyards

TU Delft

Abstract

DAMEN tugs can be found in nearly any port or terminal around the world. Operating in ports and terminals requires the tugs to be highly efficient in ship handling in order to quickly maneuver larger vessels. To predict the escort capabilities of a tug, DAMEN has developed the computer program DAMEN TUGSIM. Since the tool is becoming a decisive tool in the design process, DAMEN wants to strengthen their confidence in the simulation tool TUGSIM by gaining more understanding related to the thruster performance. The goal of this study was to quantify and increase understanding into the following regions: Thruster performance in oblique flow; Hydrodynamic interaction effects encountered between thrusters; Hydrodynamic interaction effects encountered between the thruster and hull. Recently performed model tests of a RSD (Reverse Stern Drive) tug provided the opportunity to gain insight into these topics and to derive prediction models. Mathematical models are developed and finally implemented in TUGSIM. Implementation of the new models enabled to harvest new insight into escort capabilities of the RSD tug, especially into the braking capabilities.

Contents

List of Symbols

Roman Symbols

A_{prop}	Propeller disk area	[m^2]
A_o	Propeller disk area	[m^2]
A_R	Propeller race disk area	[m^2]
A_A	Advance area	[m^2]
C_Q	Torque coefficient	[-]
C_T	Thrust coefficient	[-]
C_X	Longitudinal (thrust) force coefficients	[-]
C_Y	Transverse (side) force coefficients	[-]
C_N	Drag coefficient	[-]
D	Diameter of Propeller	[m]
D	Drag	[kN]
D_D	Diameter of Propeller	[m]
D_R	Diameter of Propeller	[m]
F_x	Force in direction of x-axis	[kN]
F_y	Force in direction of y-axis	[kN]
F_T	Thrust force	[kN]
e	Minimum distance between race area and propeller area	[m]
J	Advance velocity coefficient	[-]
k	Race coefficient	[-]
K_T	Thrust coefficient open water	[-]
K_s	Side force coefficient open water	[-]
L	Lift	[kN]
L_{CLD}	Distance between centre of rotation and leading edge of duct	[m]
L_{CTD}	Distance between centre of rotation and trailing edge of duct	[m]
M_x	Moment around x-axis	[kNm]
M_z	Moment around z-axis	[kNm]
$\dot{m}$	Mass flow rate	[kg m/s]
n	rotational speed of propeller	[rpm]
P	Pitch of propeller blade	[m]
P/D	Pitch ratio	[-]
R	Radial load	[kN]
R_V	Velocity ratio	[-]
S	Towline force	[kN]
s	Thruster spacing	[m]
T	Thrust force	[kN]
t	Thrust deduction factor	[-]
T_E	Effective Thrust force	[kN]
T_{real}	Actual Thrust	[kN]
T_0	Open water thrust	[kN]
V	Speed	[m/s]
V_{ax}	Effective axial velocity component of free stream	[m/s]
V_{axr}	Axial velocity component in the wake of the propeller race	[m/s]
V_{ind}	Induced velocity by propeller	[m/s]
V_o	Velocity at propeller disk	[m/s]
V_r	Relative velocity	[m/s]
V_R	propeller race velocity	[m/s]

V_s	Speed of Vessel	[m/s & kn]
w	Wake fraction	[-]
x_s	Starting condition input parameter	[-]
x_{Hull}	Hull input parameter	[-]
x_{Skeg}	Skeg input parameter	[-]
x_{Prop}	Propulsion input parameter	[-]
x_{Nozz}	Nozzle input parameter	[-]
x_{Rud}	Rudder input parameter	[-]
X	Axis in X-direction	[-]
x_R	ordinate of the race trajectory in x-direction	[-]
Y	Axis in Y-direction	[-]
y_R	ordinate of the race trajectory in y-direction	[-]
Z	Axis in Z-direction	[-]

Greek Symbols

α	Orientation of the thrust w.r.t free stream coordinate system	[deg]
β_H	Drift angle w.r.t free stream coordinate system	[deg]
β_P	Hydrodynamic pitch angle (i.e. Advance angle)	[deg]
β_{PR}	Advance angle race	[deg]
δ	Thruster angle	[deg]
ϕ	Heeling angle	[deg]
γ	Towline angle with respect to ship coordinate system	[deg]
θ	Angle of attack (i.e. Incidence Angle) $\theta = \beta + \delta$	[deg]
λ_D	Coefficient for proportion of the thruster affected by the race	[-]
λ_R	Coefficient for proportion of the thruster affected by the race	[-]
ζ	Orientation of the inflow with respect to the free stream	[deg]
ζ_0	Orientation of the outflow with respect to the free stream of the leading thruster	[deg]
ξ	Proportion of the thruster affected by the race	[-]
ρ	Density of water	[kg/m^3]
τ	Towline angle with respect to free stream coordinate system	[deg]

Abbreviations

AMS	Australian Maritime College
ASD	Azimuthing Stern Drive
ATD	Azimuthing Tractor Drive
F	Free stream fixed
kn	Knots
kN	Kilo newton
l	Leading thruster or edge
MAE	Mean absolute error
NFSI	Ship Research Institute of Norway
PSA	Port side aft
PS	Port side
SBA	Starboard side aft
SB	Starboard side
RMAE	Relative mean absolute error
RSD	Reverse stern drive
RPM	Rounds per minute
RMSE	Root Mean Square Error
sh	ship fixed
t	Trailing thruster or edge
th	thruster fixed
tl	Trailing - leading thruster

Sign convention

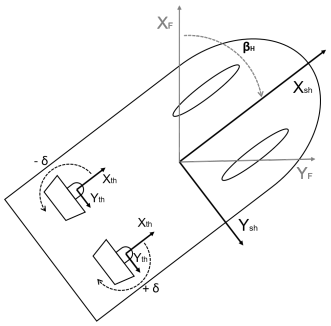

Figure 1: Rectangular coordinate system vessel

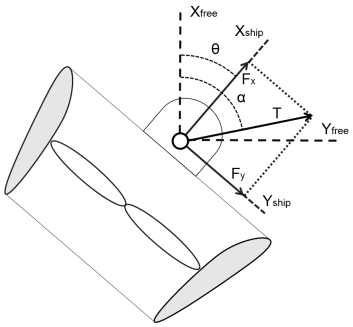

Figure 2: Rectangular and polar coordinate system thruster

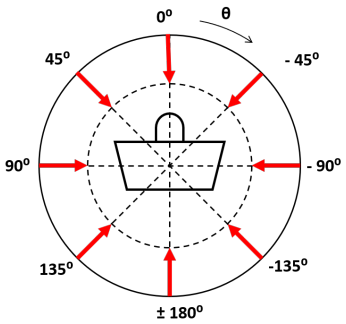

Figure 3: Convention angle of attack (incidence angle) θ

1 Introduction

1.1. Introduction TUGSIM

In its 90 years of existence, DAMEN Shipyards has become an established brand in the global market of tugs. DAMEN tugs can be found in nearly any port or terminal around the world. Operating in ports and terminals requires the tugs to be highly efficient in ship handling in order to quickly maneuver larger vessels in limited maneuvering space. The key features of a tug are the towing and escorting performance. To predict the escort capabilities of a tug, the DAMEN Research & Development department (R&D) has developed the computer program DAMEN TUGSIM. The objective of the tool is to generate predictions of the escorting forces in a quick fashion, meaning that with a minimum amount of input, a reasonable estimate should be given. This enables a designer to have a tool to qualitatively and quantitatively study the influence of different tug configurations and optimize the design in an early stage. Since the tool is becoming a decisive tool in the design process, DAMEN wants to strengthen their confidence in the simulation tool TUGSIM by gaining more understanding related to the thruster performance from experimental tests.

Figure 1.1: Illustration of an escorting operation

1.2. Problem description

TUGSIM is the simulation program which calculates the effective pull of a tug (i.e. towline force) in escorting operations. The towline force results from the quasi-static equilibrium of the propulsion forces and the hydrodynamic forces of the hull and appendages. The mathematical model is based on a modular structure, i.e. forces acting on the hull, propulsion and appendages are evaluated separately. Interaction between these elements are determined by separate algorithms. A good model and understanding of these forces is considered to be essential to make a good and reliable calculation of the escorting performance.

The main problem to be addressed in this thesis is the reliability of the prediction of the thruster performance in escort conditions. Conditions that are characterized by large drift angles and high vessel speeds. For these conditions a greater consideration needs to be given into three regions:

1. The first region of interest relates to understanding of the thruster performance in oblique flow. The oblique angle of the inflow is created by sailing at drift and the very nature of the thruster, namely its capability of rotating while operating.
2. The second regions of interest arises from the tugs being fitted with multiple thrusters. The thrusters operating in close vicinity interact, resulting in a potential loss of thrust.
3. The third region of interest lies in the hydrodynamic interaction effects that are encountered by the thruster and hull in escort conditions. The complex interaction phenomenon can potentially lead to significant reduction of the thruster performance and consequently the escorting performance.

The abovementioned regions haven't yet been thoroughly investigated and are therefore not well understood. Because of this, it is unknown whether TUGSIM provides a reliable and good prediction of the escorting performance. Extensive model tests are performed at MARIN. These tests give the possibility to gain insight into the abovementioned topics.

1.3. Research objective

In view of the problem statement presented in the previous section the objective of the current work is formulated as:

The goal of this thesis is to quantify and increase the understanding of the azimuthing thruster forces and hydrodynamic interaction effects of a tug in escorting conditions in order to enhance the reliability of the TUGSIM calculation.

The main objective is divided in the following sub-objectives:

- Assess the agreement of the thruster force model with experimental data and identify which phenomena related to the thruster performance are not captured by TUGSIM
- Investigate the experimental data and identify relations and trends in the measured thruster forces
- Develop a generic quasi-static thruster force model that suitably predicts the relevant trends
- Determine the impact of the new models on the escorting performance by means of a TUGSIM case study

1.4. Research approach

To systematically investigate and quantify the topics related to the thruster performance, the research is divided into the following aspects:

- Single thruster in open water to study the effect of oblique flow
- Two thrusters in open water to study the effect of thruster-thruster interaction
- Two thrusters behind hull to study the effect of thruster-hull interaction

In this research, open water is defined as a thruster operating in a flow which is not disturbed by hull or thrusters. To accomplish the objective a general research approach is set-up that is followed for each aspect. The general research approach is presented in the overview in figure 1.2.

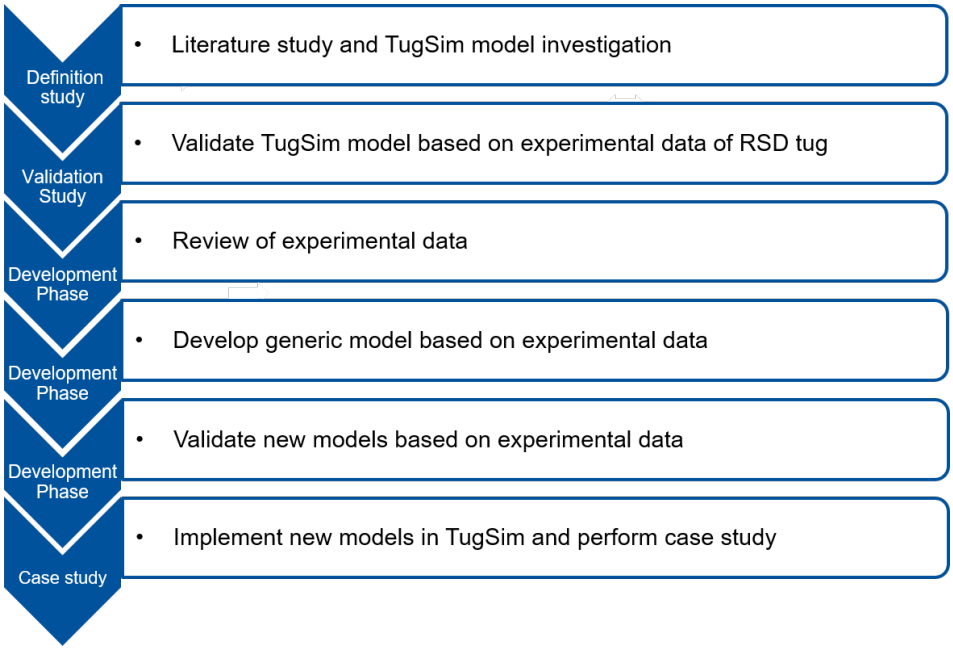

Figure 1.2: General research approach

1.5. Report outline

The general structure of this report is set-up based on the three aspects addressed in the previous section. The outline of each chapter is based on the general approach, only the TUGSIM case study is presented in a separate chapter. First, general information is provided on the topic of escorting maneuvering and tugs, followed by a description of TUGSIM. Chapter 3 presents the results of the research into single thruster in open water. In chapter 4, two thrusters in open water are discussed with main focus on thruster-thruster interaction. Chapter 5 describes the results of two thrusters in behind hull where primarily the influence of the hull is investigated in combination with the study into thruster-thruster interaction at various drift angles. Chapter 6 presents the results of the implementation of the proposed models into TUGSIM and various simulation cases. Finally, the report is finished with the conclusions, limitations of the study and recommendations.

2

TUGSIM

TUGSIM was briefly highlighted in the introduction. This chapter details a description of the prediction model in TUGSIM. First, general information is provided on the topic of escorting maneuvers and tugs.

2.1. Escort tugs

The name escort tugs is used for tugs specially designed to generate steering (i.e. transverse) and braking (i.e. longitudinal) forces to escort ships over long distances with relatively high speed. The generated towline force of an escort tug is generally higher than the force generated in bollard pull conditions (i.e. low speeds). This is in contrast to harbour tugs, which generate the highest force at low speeds. The types of escort tugs that can be found in the ports around the world are characterized by four aspects: type and location of the propulsion, the location of the skeg(s) and the location of the towing point. The main types that are build by DAMEN are shown in the illustrations below. The towing point location is indicated in the illustrations by a red arrow.

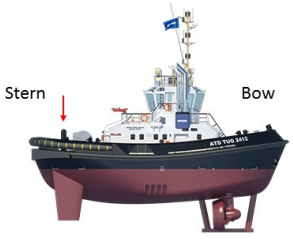

(a) ATD - Azimuth tractor tug

(b) ASD - Azimuth stern drive tug

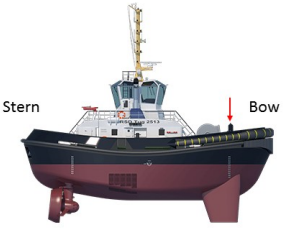

(c) RSD - Reverse stern drive tug

Figure 2.1: Overview of Escort Tug Types

2.2. Escorting modes

Escorting is defined as actively (emergency) steering, braking and controlling the escorted ship by the tug, whereby the ahead speed of the escorted ship is within a typical speed range of 6 to 12 kn. The primary categories of escorting operating modes that are being used by tug operators are defined as the direct towing method, indirect towing method and combination mode. Figure 1.1 gives an illustration of the indirect towing mode. An elaboration is given on both towing methods in the following subsections.

Escorting operations are characterized by the following aspects:

- High speed
- Large drift angles
- High heeling angles
- Oblique inflow of the thrusters

2.2.1. Direct towing mode

In the direct towing mode [14], the thrust force is directly applied to generate the towline force, whereby the hydrodynamic lift and drag forces play no significant role. This method is used when only a braking force is required to slow down the escorted vessel. The two direct methods are reverse arrest and transverse arrest. In a reverse arrest, the azimuth drives apply a force directly opposed to the direction of motion. Transverse arrest involves orienting the azimuth thrusters perpendicular to the flow to achieve that they are both propelling water outward at 90°. The latest is highly effective at higher speed.

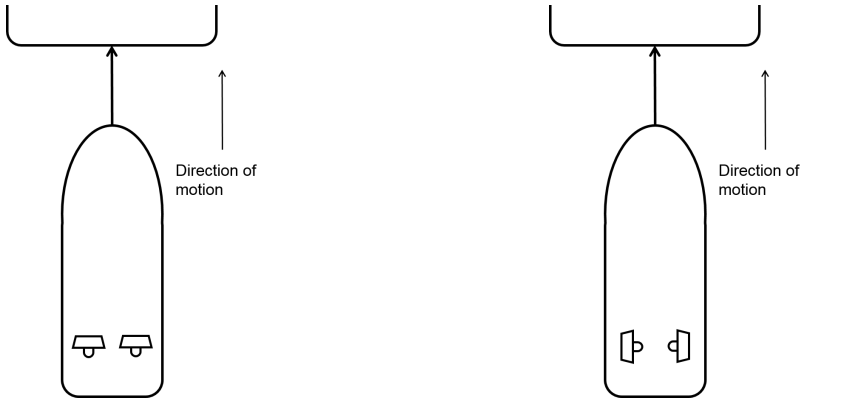

(a) Direct mode: reverse arrest (b) Direct mode: transverse arrest

Figure 2.2: Direct towing mode

2.2.2. Indirect towing mode & combination mode

The indirect towing mode is the method to apply steering and braking forces to an escorted ship, especially at higher speed. The traditional mode involves utilizing the hydrodynamic characteristics of the tug's hull and appendages to generate lift and drag forces by orienting the tug at non-zero yaw angles to the direction of motion (also referred to as drift angle). In "basic" indirect mode the towline force is generated primarily by the hydrodynamic forces acting on the hull and skeg, with the thrust used solely to maintain the desired drift angle. In "powered" indirect mode the transverse component of thrust is used to maintain the desired drift angle, while a significant longitudinal component of thrust is applied in forward direction of the tug and enhances the steering force. This mode is usually used to create maximum steering forces at high speeds. The "combination mode" is a combination of the direct mode and indirect mode. In combination mode the same principle as for the "powered" mode is applied, except that the longitudinal component of thrust is applied in aft ward rather than forward

direction. This mode is often used at high speed to create high braking forces. Illustrations of the towing modes can be found in figure 2.3.

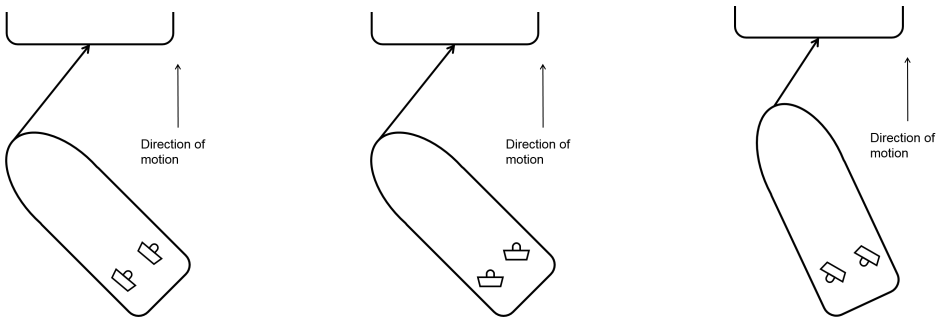

(a) Basic (b) Powered (c) Combination

Figure 2.3: Indirect escorting mode

2.3. TUGSIM

The computer program TUGSIM is a force-equilibrium-simulation program which is developed by DAMEN in order to predict the effective pull that a tug can deliver in bollard pull and escorting conditions. The effective pull is the resultant from the equilibrium condition reached between the propulsion forces and the hydrodynamic forces of the separate subcomponents. The general structure of the simulation tool is shown in figure 2.4, where x_s denotes the starting condition input parameters.

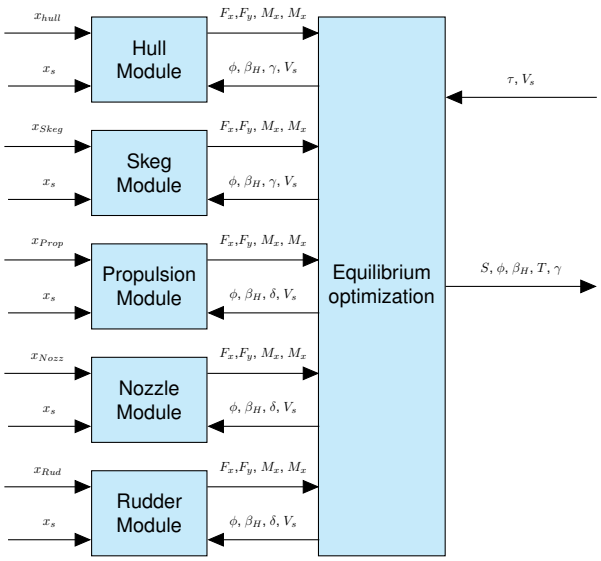

Figure 2.4: General block diagram of TUGSIM simulation tool

The block diagram is build up from various sub-modules and a main module called equilibrium optimization. The sub-modules contain the mathematical model of the various subcomponents. These subcomponents are the skeg(s), rudder(s), propulsion unit(s) and the hull. The components can be of any number and size and can be placed anywhere on the hull. This flexible modular approach results in a versatile software tool that can be used for both existing and future designs. Description of the sub-modules can be found in the sections below and in program description written by Timmers [25].

The main module contains the force and momentum equilibrium of the vessel. The main assumption is that any towing operation in bollard pull condition or at speed can be viewed as a quasi-static equilibrium. Tug boats in escort operations need to produce a constant force for a significant long

period in order to break or steer the escort vessel. These conditions may therefore be assumed to be quasi-static. Transient behavior, such as accelerations and behavior between equilibria, are not of importance in this tool and are not included. The quasi-static equilibria are expressed in four equations:

$$\sum F_x = F_{hull_x} + F_{skeg_x} + F_{Nozz_x} + F_{Rudder_x} + F_{Prop_x} + F_{Tow_x} = 0 \tag{2.1}$$

$$\sum F_y = F_{hull_y} + F_{skeg_y} + F_{Nozz_y} + F_{Rudder_y} + F_{Prop_y} + F_{Tow_y} = 0 \tag{2.2}$$

$$\sum M_x = M_{hull_x} + M_{skeg_x} + M_{Nozz_x} + M_{Rudder_x} + M_{prop_x} + M_{Tow_x} = 0 \tag{2.3}$$

$$\sum M_z = M_{hull_z} + M_{skeg_z} + M_{Nozz_z} + M_{Rudder_z} + M_{prop_z} + M_{Tow_z} = 0 \tag{2.4}$$

The F_z and M_y equilibria are not included, because the effect of trim and draught variations on the towline force is considered to be insignificant. The second assumption is that the effect of current, wave and wind on the tug's equilibrium are ignored. The above equilibria are set-up for a towing condition, but a set of variables is unknown. These variables are called the linking variables and link the sub-modules with the main module. TUGSIM uses an iterative mathematical procedure to obtain the values of these variables corresponding to the equilibria at which the maximum escorting performance are achieved. A description of this procedure is described in Timmers [25].

2.3.1. The propulsion model

The function of a propulsion system is to generate a thrust force to overcome the resistance of the hull and move at a desired speed. The main system components of a propulsion system are: the engine, transmission and propulsor. Tugs are generally equipped with two types of propulsors: fixed ducted propellers or azimuthing ducted propellers. Computing the propulsor thrust force requires to go through the complete propulsion chain that includes all system components with their specific power and efficiencies [15]. In TUGSIM, a simplified propulsion chain is modelled and only includes the propeller model, since a more complex model would require high computational power and decrease the advantage of the simulation tool. The general structure of the tug's propulsion simulation model is shown in the block diagram in figure 2.5.

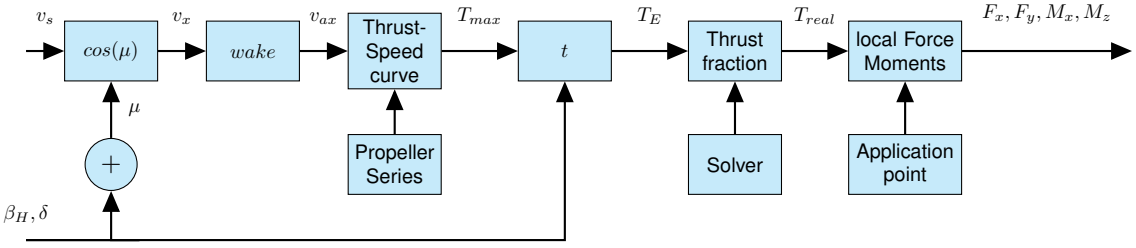

Figure 2.5: Propeller model block diagram

The relevant blocks for this study are explained in the subsections below. The above block diagram is identical for the port side and starboard side thruster. Only the determination of the application point of the thrust force is different for the thrusters. It is however assumed that the characteristics of the thrusters are always identical.

The explanation of the blocks is not publicly available.

2.3.2. The nozzle model

(Not publicly available)

3

Case study

The Reverse Stern Drive (RSD) Tug "2513" is used as case study throughout this thesis. Extensive experimental model tests were performed of the new designed RSD Tug 2513 in order to gather information of the propulsive performance and hull forces in typical escorting operations. The information can be used to quantify and increase understanding of aspects related to thruster forces in various escorting conditions.

This chapter provides a description of the vessel under investigation. Next, the experiments are explained. Finally, a short description of the used coordinate systems and graphical representation method are presented.

3.1. Reverse Stern Drive (RSD)

The RSD Tug 2513 is the result of years of research and development by DAMEN. The design combines elements of ATD and ASD tugs to create a class of vessel that effectively has two bows, enabling it to always operate the bow first. The result is a tug that is equally effective at bow assists and stern assists.

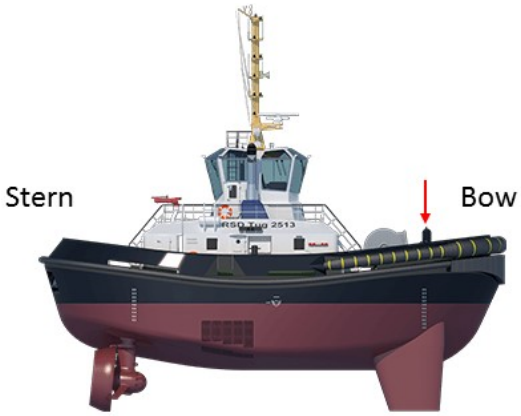

Figure 3.1: Reverse stern drive (RSD) tug, red arrow = location towing point

Two large wing shaped profiles, also know as skegs, are located at the bow. The vessel is equipped with two azimuthing thrusters located at the aft of the vessel. This thruster units have the ability to rotate 360 degrees around its z-axis and can therefore deliver full thrust in any required direction.

3.2. Model experiment

(Not publicly available)

3.3. Model test uncertainty

(Not publicly available)

3.4. Processing measurement data

The primarily focus of this study is on the thruster forces. These forces are measured on the thruster unit, meaning that the forces are presented in a ship fixed axis system. To gain more insight, forces are converted to thruster fixed or free stream axis system by means of the rotation matrix. The rotation matrix is defined as:

$$\begin{bmatrix} X \\ Y \end{bmatrix} = \begin{bmatrix} \cos\theta & -\sin\theta \\ \sin\theta & \cos\theta \end{bmatrix} \begin{bmatrix} x \\ y \end{bmatrix} \tag{3.1}$$

Depending on the angle, forces are rotated to various axis systems.

The measurement data is presented in various coordinate systems, namely cartesian and polar coordinate systems. The measurement data in polar coordinates can be presented in polar diagrams. This representation technique is favoured since it facilitates to compare thruster characteristics at similar incidence angles. To demonstrate this type of graphical representation, an example is provided in figure 3.2.

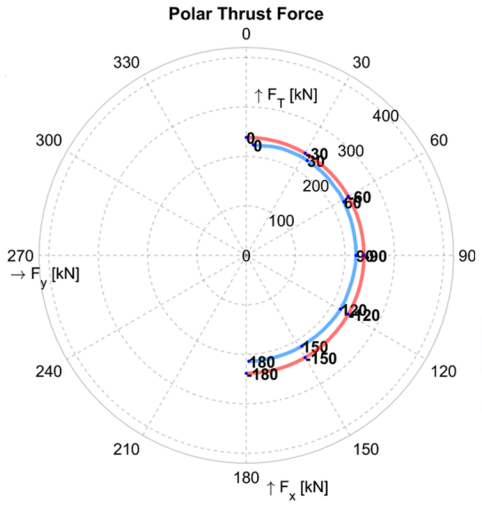

Figure 3.2: Polar diagram example

The angular coordinate specifies the direction of the thrust force with respect to the free stream and is defined as

$$\tan\alpha = \frac{F_y}{F_x}, \tag{3.2}$$

where F_y and F_y are the traversal force and the axial forces respectively. The radial coordinate defines the absolute thrust. The absolute thrust is defined as:

$$T = \sqrt{F_y^2 + F_x^2}. \tag{3.3}$$

An additional variable is added to the graph, namely the number indicated in bold. The number represents the incidence angle on the thruster with respect the free stream. The angle is a combination of the drift and thruster angle. In case the incidence angles are equal to the angular coordinate in the diagram, it means that the force is directed in the direction of the thruster. The incidence angle is defined as

$$\theta = \beta + \delta, \tag{3.4}$$

where δ and β is the steering angle and drift angle respectively.

4

Single thruster

This chapter addresses the first aspect of interest: a single thruster operating in open water. The following is presented in this chapter:

- Validity of TUGSIM based on experimental data
- Results of the investigation into the thruster performance in open water based on experimental data and literature
- An enhanced model that can adequately predict the azimuthing thruster forces

In this work, thruster performance is defined by a longitudinal F_x and transverse F_y (i.e. side) force component. These components can be combined to a single thrust, denoted as T. The orientation of the thruster forces is illustrated in figure 4.1.

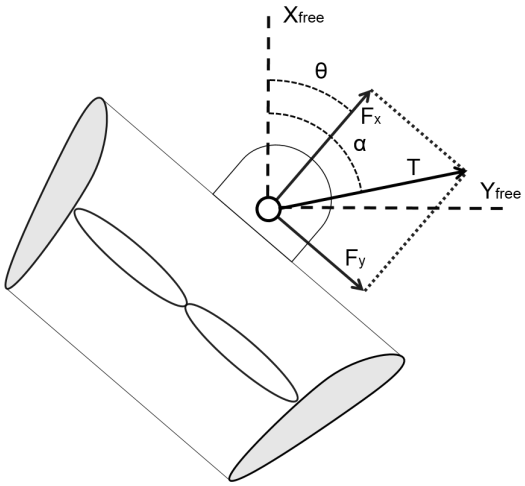

Figure 4.1: Illustration of thruster forces

4.1. Validation study

(Not publicly available)

4.2. Investigation of single thruster performance in open water

To better understand the behaviour of a single thruster in open water, the experimental data is investigated. The main focus lies on the effect of oblique flow on the thruster performance, especially at higher speeds.

Figure 4.2 presents the experimental data in the commonly used four quadrant diagram representation. To derive the diagram, the thruster fixed forces are non-dimensionalized with respect to the propeller revolution, the propeller diameter and the advance speed. Only the first and fourth quadrant are considered as only positive rotational speeds are tested in the experiment. The thrust forces are discussed first, followed by the side force.

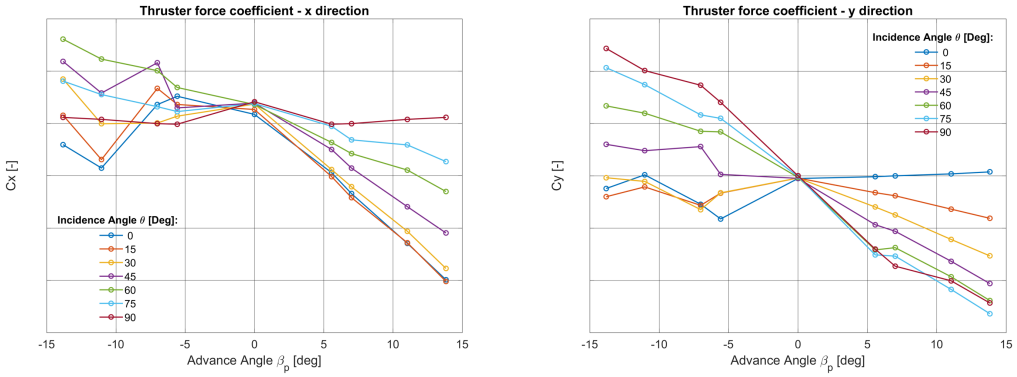

(a) Thruster fixed thrust force coefficient

(b) Thruster fixed side force coefficient

Figure 4.2: First and fourth quadrant diagram for various angles of attack, starboard thruster

4.2.1. Thrust investigation

The curves in figure 4.2a show that the thrust coefficient is a decreasing function of the advance angle. The thrust coefficient is an increasing function of the incidence angle. Except for an incidence angle of 90 degree, the thrust coefficient is almost constant and remains close to the thrust at bollard pull.

At negative advance angles fluctuations in thrust are observed. Negative flow conditions are characterized by large angles of attack and high torque, with the possibility of stall and unsteady flow [5]. In these conditions there exist not only blade stall, but also separation of flow from the nozzle and propeller blade. The unsteady nature of such flow field can create significant thrust fluctuation, according to Brandner [3]. The fluctuations in the data for negative advance angles can therefore be attributed to these hydrodynamic phenomena.

To investigate the trend and the contribution of all components to the total thrust, numerical studies by Pavliouglou [20], Zhang [29] and Bulten [4] are used. In specific the study by Pavlioglou is useful since a large range of incidence angles is analyzed. The results of Pavlioglou are presented by the open water parameters $K_T(J, \theta)$ in figure 4.3. The thruster unit is divided into a propeller, nozzle and pod & shank component. Only positive incidence angles are analyzed. First of all, it can be observed that trends are similar to the trends observed in the experimental data.

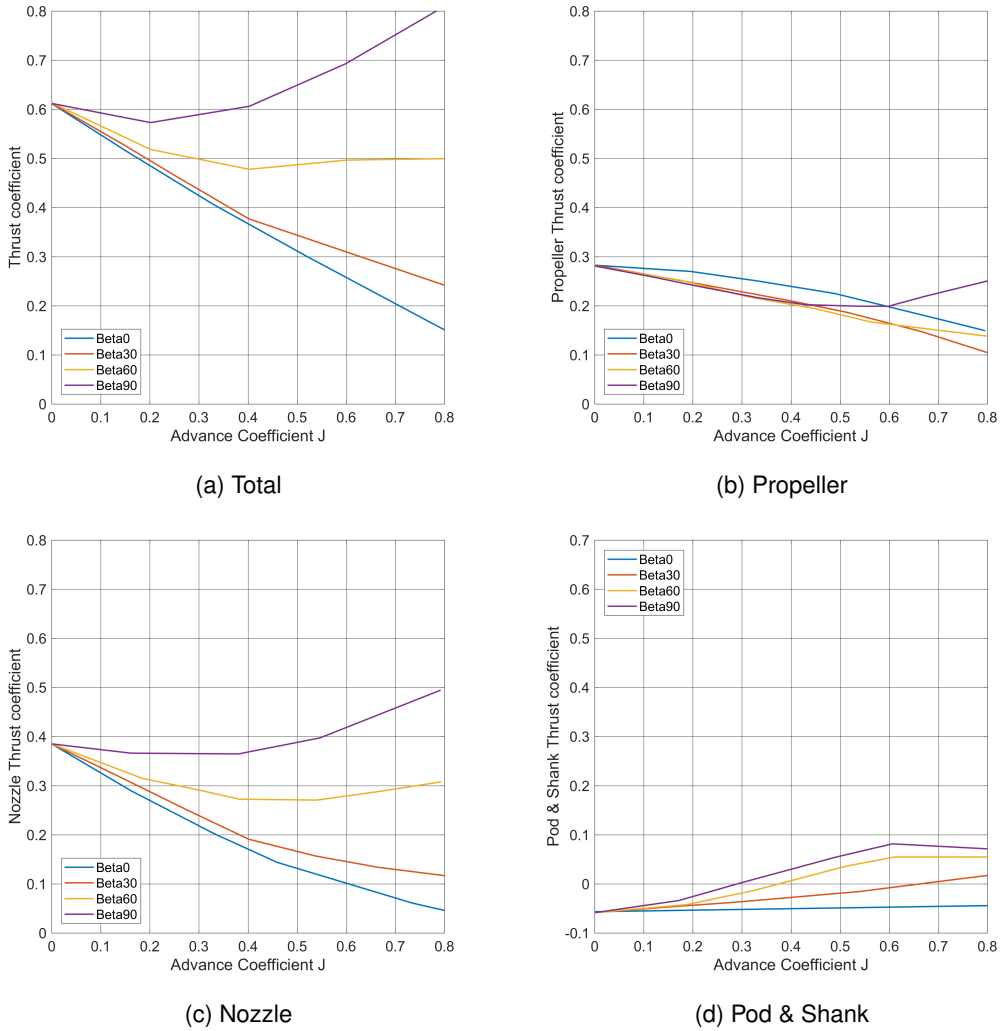

(a) Total

(b) Propeller

(c) Nozzle

(d) Pod & Shank

Figure 4.3: Thrust force coefficients by Pavlioglou [20]

From figure 4.3a, it is evident that throughout the whole range of J the thrust delivered becomes significantly higher with increasing incidence angle. For small angles, the total thrust is a decreasing function of the advance angle. This trend can be explained by the operational principle of the propeller and nozzle. For incidence angles larger than 60°, the total thrust is no longer a decreasing trend. From figure 4.3, it is apparent that the driving component for the value of the total thrust is the nozzle.

This behaviour of the nozzle thrust lies thus in its operational principle. During operation of the propeller, water is forced into the nozzle. As the water follows the shape of the nozzle, the flow is accelerated along the nozzle. According to the second law of Newton [27], the acceleration of the flow creates a reaction force applied on the nozzle, also known as lift and drag. Lift and drag result partly in a radial load pointing towards the center of the nozzle, and partly in axial component which is perceived as thrust. Lift and drag highly depend on the angle of attack. Hence, anything that can affect the angle of attack has an effect on the amount of thrust delivered by the nozzle. The axial velocity of a thruster unit is a factor that greatly affects the angle of attack.

In bollard pull conditions, the vessel speed is zero and axial velocity is by definition equal to zero. Still flow is accelerated by the operating propeller and forces water into the nozzle. A very high angle of attack is experienced by the nozzle and consequently high delivered nozzle thrust. A sketch of a nozzle section in bollard pull conditions is displayed in figure 4.4a. With increasing speed, the flow is superimposed with an incoming velocity and the angle of attack becomes lower as can be seen in

figure 4.4b. A reduced angle leads to a decreased thrust delivery of the nozzle. This explains the decreasing function as function of the advance angle for small incidence angles.

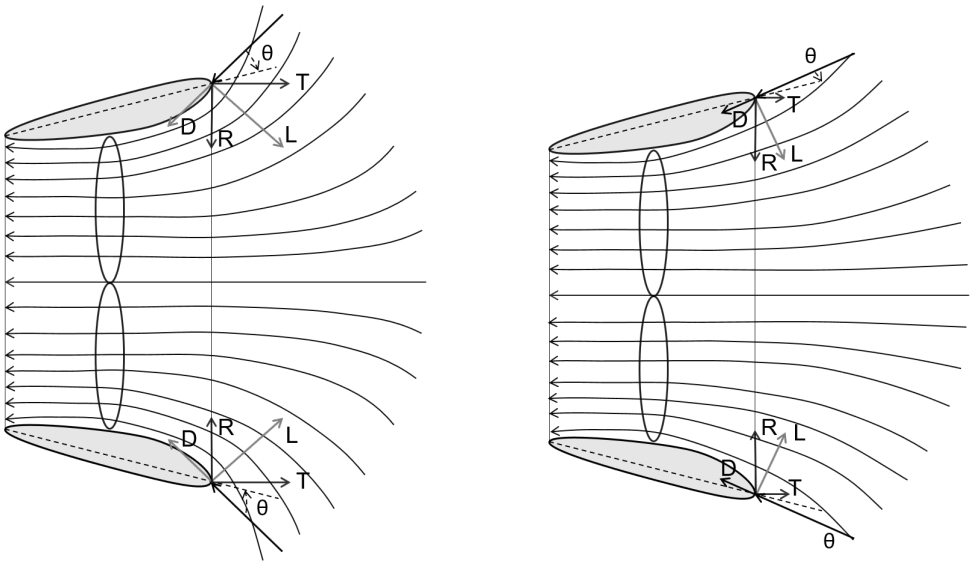

(a) bollard pull (b) At speed

Figure 4.4: Illustration of stream lines in bollard pull condition

With increasing incidence angle, the velocity in direction of the thruster (i.e. axial component) reduces and the angle of attack increases. The situation is illustrated in figure 4.5. The impact of an increased angle of attack results in increased thrust by the nozzle. For small incidence angles, thrust remains a decreasing function of the advance angle. In case of 90°, the delivered thrust exhibits an increasing behaviour as the axial velocity component is small. Therefore a change in velocity has a marginal effect on the axial velocity and consequently on the thrust. This explains the almost constant thrust at incidence angle 90° in figure 4.2.

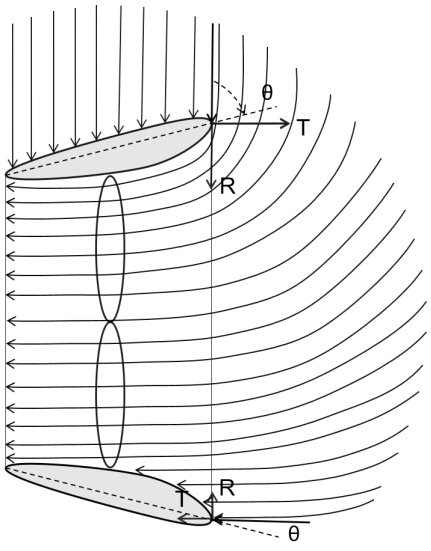

Figure 4.5: Illustration of stream lines in oblique flow

Figure 4.2 shows that thrust of the thruster unit can be higher at negative incidence angles in comparison to positive angles. Again, this can be explained by the operational principle of the nozzle. At negative inflow the angle of attack with respect to the nozzle is large and results in high thrust. Torque

of the propeller can be high in such conditions which may lead to overloading of the engine. In reality, the thruster may therefore not always be able to generate the indicated amount of thrust as the revolution needs to be reduced to maintain in the engine envelope.

The study into the operational principle of the nozzle demonstrated that the angle of attack controls the amount of thrust delivered by the nozzle and is affected by the the axial velocity towards the nozzle. Hence, thrust can be determined by determining the axial velocity. This principle is used in TUGSIM. Validation indeed confirmed that using this methodology provided a correct estimate of the thrust delivered by the thruster unit in both straight and oblique flow. Therefore it is not necessary to develop a new model.

4.2.2. Side force investigation

Along with the thrust, a side force (F_y) is generated on the thruster unit when operating in oblique flow. The side force curves in figure 4.2 show that the magnitude of the side force is an increasing function of both the advance angle and incidence angle. For straight flow, the value of the side force remains almost zero, expect for negative flow conditions. It was expected that the side force remains small as the side force is cancelled out due to the axis-symmetric shape of the nozzle and the symmetry of the flow around the structure of the unit. The significant values observed in negative flow conditions can generally be attributed to the unsteady nature of flow field and may therefore not always be observed.

The study by Pavlioglou can again be used to distinguish the individual impact of the various components in the overall side force trend. The graphs are presented in figures 4.6 and 4.7. First of all, it can be observed that trends are similar to the trends observed in the experimental data.

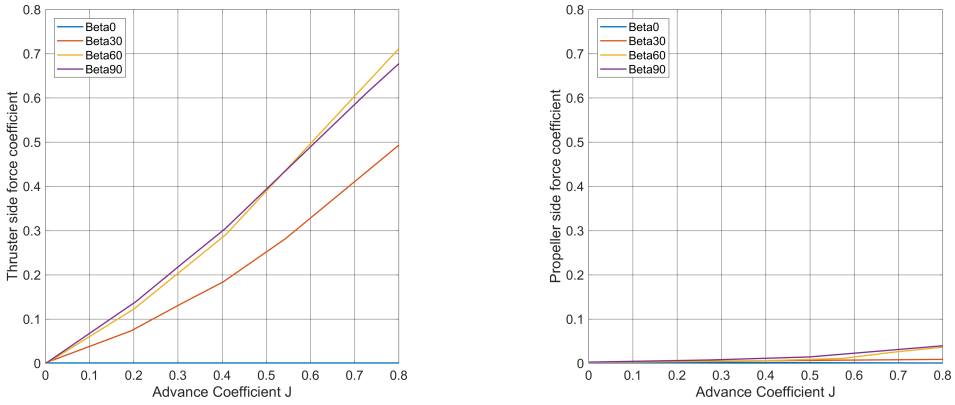

(a) Total (b) Propeller

Figure 4.6: Side force coefficients by Pavlioglou [20]

Secondly, it seems that the impact of the propeller in the overall trend is not the driving component of the total side force. The combined contribution of the pod and shank is even bigger than that of the propeller, as can be observed in 4.7b. The contribution by the propeller to the total side force is small due to the flow straightening effect of the duct on both the propeller in and outflow. For an open thruster, the contribution of the propeller will be much higher [2]. Finally, the nozzle seems to have the highest contribution of all components in the total side force, as presented in figure 4.7a. It is an increasing function of both the advance coefficient and incidence angle. The incremental behaviour applies for all incidence angles up to 60°. The magnitude of the side force on the nozzle seems to be unaffected by any further increase of incidence angle beyond 60°. Similar trend is observed in the experimental data.

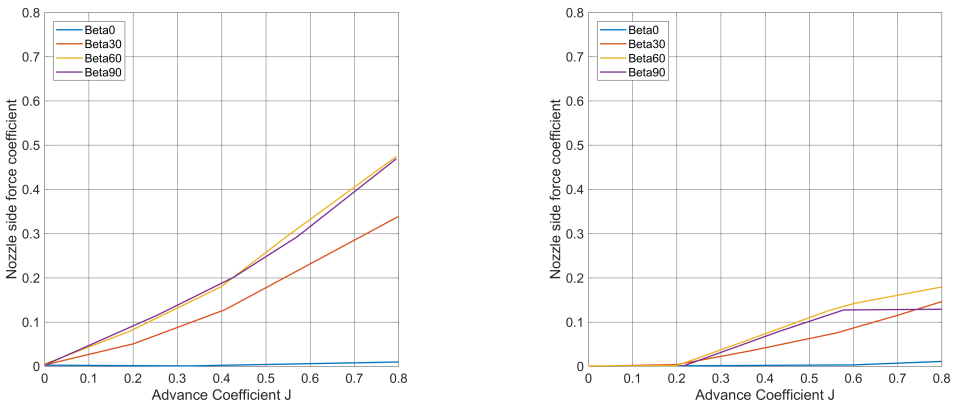

(a) Nozzle (b) Pod & Shank

Figure 4.7: Side force coefficients by Pavlioglou [20]

It can be concluded that side forces are mainly confined to the nozzle operating in oblique flow. To understand the behaviour of the side forces, insight must be gained into the flow effects related to a duct operating in a cross flow. The situation is very similar to a ducted-fan aerial vehicle, for which cross flow has a large impact on the stability of the vehicle [13] [21]. In this case a profound understanding of the aerodynamic forces is essential. It is assumed that the aerodynamic characteristics are similar to the hydrodynamic characteristics. When analyzing the forces imposed due to the incoming flow, two flow effects related to side force were identified:

1. Body drag

2. Momentum drag

Body drag is the resistance force caused by the motion of the nozzle through the water. The drag force acts in the direction of the flow velocity. This component is not associated with drag force generated by the propeller forcing water into the nozzle. In straight flow, the drag force is small due to the small projected area of the nozzle. In oblique flow, the projected area of the nozzle increases and consequently the drag force increases. The drag equation can be used to calculate the force of drag experienced by the nozzle . The drag is proportional to the square of the velocity. This relation can also be identified in figure 4.7a.

The second drag component is called the **momentum drag**. It can be explained by the operational principle of the nozzle. The operational principle was previously discussed. In oblique flow, the thruster experiences a cross flow. In the presence of the cross flow, the fluid particles need to be aligned with the nozzle, as can be seen in figure 4.5. The fluid particles must be accelerated along the shape of the nozzle creating a reaction force on the nozzle. The radial component of the reaction force is perceived as the side force. In comparison to straight inflow, particles need to be more accelerated to align it with the duct and thus creating higher loads, especially in radial direction.

Furthermore in straight inflow conditions, the radial loads are cancelled out due to axis-symmetric shape of the nozzle and symmetry of the flow around the nozzle. In oblique flow, the flow around the nozzle is asymmetrical. One part of the nozzle experiences high radial loads whereas the other side experiences low radial loads, as can be seen in figure 4.5. Consequently this results in a resultant side force on the nozzle. The phenomenon described above is also known as momentum drag [21], since drag is mainly responsible for the radial loads. The derivation of the momentum drag is later explained in section 4.3.2. From the relation can be seen that the reaction force is an increasing function of the velocity (i.e advance angle) and incidence angle. A trend that is similar to the observed in figure 4.2 and 4.7a.

4.3. New thruster forces model

A new model is developed to adequately predict the thruster characteristics using the gained knowledge and data from section 4.1 and 4.2. The new propulsion model is composed of two components:

- Longitudinal thruster force (i.e. thrust)
- Transverse thruster force (i.e. side force)

Two approaches are used to develop a prediction model of the thruster performance, namely a theoretical and empirical approach. A numerical method is not fancied since it would require too much computational effort. This is not in line with the main objective of the simulation tool of providing a tool that can generate a prediction in a quick fashion.

First, a brief summary is given of the models found in literature. Next paragraphs present the theoretical and empirical model. The section ends with a validation study by means of comparing the predictions from both models with experimental data.

4.3.1. Previous studies

Previous studies investigating the thruster characteristics have been limited to purely axial inflow conditions in which side forces are small. Some studies are conducted into the characteristics in oblique flow, but often use a numerical or experimental based approach. Bulten [4], Zhang [29] and Berchiche [2] conducted numerical studies to determine the performance of thrusters in oblique flow. From the studies insight into the behaviour of the hydrodynamic loads in oblique flow angles can be gained. The studies reveal that the nozzle absorbs much effort from the oblique flow. Pavlioglou [20] is an expansion to the work by Bulten since he expanded the research range of incidence angles from 0° to 90°. Detailed insight into the contribution of each thruster unit component is gained and underlying physical phenomena are analyzed. Results were used in section 4.2.

Detailed studies into the influence of oblique flow are conducted for open propellers by Schulten [23], Dalheim [6] and Gutche [11]. The studies presented an analytical treatment of the propeller with oblique flow. These analytical models are not relevant for the ducted propeller since the propeller is relatively unaffected by oblique flow, as was concluded in section 4.2.

Nienhuis [18], Minaas [17] and Oosterveldt [19] experimentally tested azimuthing thrusters. The latter attempted to represent the characteristics at various incidence angles by extrapolating a Fourier series representation of conventional straight inflow four quadrant measurement. Using this approach, it is not possible to predict the thruster side force. The experimental data of the mentioned studies is published and can be used for validation.

Brandner presents some studies that propose a theoretical method to predict the side force, but concludes that no theoretical method is adequate in predicting the characteristics yet. The applicability range (i.e. incidence and advance angles) of the methods is mainly the limiting aspect. Therefore Brandner used an empirical approach and derived the thruster characteristics directly from experimental results. The characteristics are presented by a mathematical model which is a function of the advance angle and incidence angle. Unfortunately, the mathematical method is not presented in his work.

Application of ducted propellers is also used for vertical take-off and landing (VTOL) aerial vehicles. A major operational problem of ducted propeller vehicles is precise control when flying in crosswinds and turbulent conditions in general. Cross wind has a large impact on stability, especially due to the presence of the duct. Pflimlin [21], Johnson [13] and Gelhausen [8] describe the underlying physical phenomena and present an analytical method to account for the influence of cross winds in the design process. In essence, the physical phenomena of an aerial ducted fan and a ducted propeller in water are very similar. The work by Pflimlin can help in determining the influence of oblique flow and determination of the side forces.

4.3.2. Theoretical side force model

According to the findings in section 4.2, side forces are mainly confined to the nozzle. The imposed load on the nozzle is divided into:

- Nozzle body drag
- Momentum drag

A sketch of the components is illustrated in figure 4.8. The **first** component is the result of the nozzle subjected to a water flow. An object in relative motion w.r.t. a fluid is subject to an hydrodynamic force that can be decomposed into a lift and drag. The magnitudes of the lift and drag depend on the angle of attack between inflow direction and chord line of the nozzle profile. To describe the lift and drag, a lift and drag model is included. The current version of TUGSIM already includes a lift and drag curve. The curve is used to predict the body drag by the nozzle.

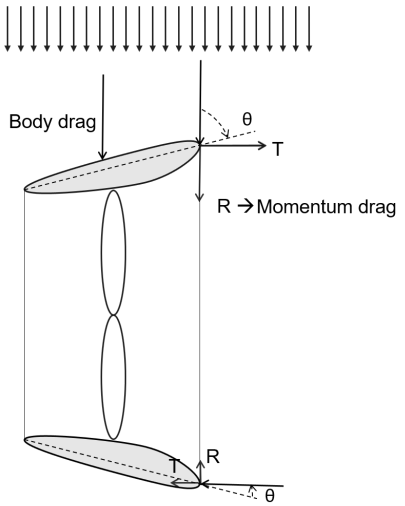

Figure 4.8: Illustration of body drag and momentum drag

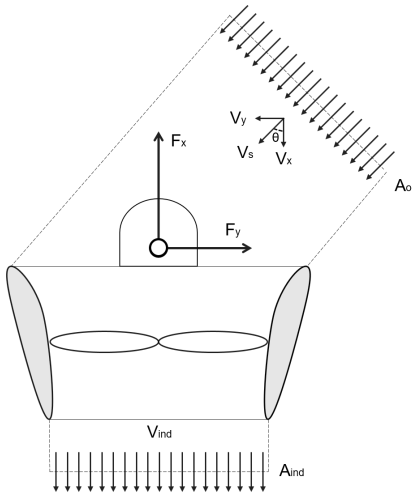

Figure 4.9: Illustration of control volume

The **second** component is the momentum drag. This type of drag is created in presence of a cross wind. The nozzle must supply a force to the incoming flow to align it with the duct. This creates a reaction force, known as momentum drag, on the nozzle. The momentum drag can be quantified by applying linear momentum theorem for a two-dimensional, friction-less and incompressible flow [13]. A control volume is defined enclosing thruster upstream and downstream part, as shown in figure 4.9. The momentum theorem for the closed surface yields [27]

$$\sum F = \oint_{CS} \rho V(V \cdot n) dS = \oint_{S_{ind}} \rho V(V \cdot n) dS + \oint_{S_o} \rho V(V \cdot n) dS = \sum (\dot{m}V)_{out} - \sum (\dot{m}V)_{in}, \quad (4.1)$$

where $\dot{m}$ is the mass flow through the duct and V is the velocity. The flow is defined by the amount of thrust generated by propeller and can be determined by

$$\dot{m} = \rho A V_{ind}, \quad (4.2)$$

where the induced velocity V_{ind} can be defined based on the amount of thrust

$$V_{ind} = \sqrt{\frac{T}{\rho A_{prop}}}. \quad (4.3)$$

From the continuity equations follows that

$$\dot{m_{in}} = \dot{m_{out}} = \rho A V_{ind}. \quad (4.4)$$

The momentum in y-direction can now be written as

$$F_y = (\dot{m}V)_{out} - (\dot{m}V)_{in} = \rho A V_{ind} \cdot V_{ind-y} - \rho A V_{ind} \cdot V_y \tag{4.5}$$

where V_{ind-y} and V_y are the lateral velocity components. Since the induced flow by the propeller is axial, lateral velocity V_{ind-y} is equal to zero. The force in y-direction (i.e side force) leaves

$$F_y = -\rho A V_{ind} \cdot V_y. \tag{4.6}$$

The above expression is included in the new thruster model.

4.3.3. Empirical side force model

The purpose of this paragraph is two-fold: to create a prediction model that accurately recovers measured side force data for those thrusters for which measured data is available, and to further provide reasonable side force predictions for the remaining thruster for which no measured data is available.

An empirical model is developed by means of a regression analysis based on experimental data sets. First the modelling process is described and finally the results are presented.

4.3.3.1. The modelling process

Building a model based on experimental data is depicted in the following stages:

- Stage 1: Selecting and preparing the data
- Stage 2: Choosing a modelling approach
- Stage 3: Performing the regression analysis and model testing

Stage 1: Selecting and preparing the data
The new model is directly derived and validated with the following experimental data:

- Captive test RSD [12]
- Oosterveld and van Oortmerssen [19], Marin Kaplan 4-70 with 19A nozzle, P/D = 1.0
- Brandner [3], AMC Kaplan 4-70 with 19A nozzle, P/D = 1.2
- Minaas and Lehn [17], NFSI P-927 with 19A nozzle, P/D = 0.9

To derive and validate the model the above data sets are divided into a training data set and a data validation set. It is desired to have a model available that is applicable for the large range of advance and incidence angles. The range of the captive RSD experiments is limited in advance angles. To prevent extrapolation, it is not desired to use this experiment to train a model. Since MARIN investigated the characteristics for the complete range of angles, this data set is used to derive the model. Although the complete range of advance angles -90° to 90° is measured, only the range between -30° and 30° degree, where the thruster forces have the largest impact on the tug performance [3], is used. The remaining data sets are used to validate and assess the performance of the model.

Stage 2: Choosing a modelling approach
A prediction model of the side force is created via a regression analysis. The basic idea of a regression analysis is to develop a model for given responses in form of equation 4.7 [26]:

$$\hat{y}(x) = f(x) + e, \tag{4.7}$$

where $\hat{y}(x)$ is the desired function value at a location x, $f(x)$ is the approximation model given by a certain function and e is the prediction error. The function $f(x)$ is a black box which obscures the physics that converts x into an output y. The evaluation of the black box takes the form of a physical experiment. The challenge is to find a best guess for the black box based on these known observations. There are various generic modelling methods $f(x)$ available to express the physical experiment [9]. A few traditional methods are listed below:

- Linear regression method
- Polynomial regression method
- Fourier analysis

The last two techniques are widely applied in propeller series application since the relationships are typically non-linear. For instance, MARIN used a Fourier analysis to describe the four quadrant experimental data. The polynomial functions are widely applied to mathematically express the open water measurement data.

An alternative method to predict the unknown values is the Kriging regression method [10] [16] [26] , which is often used for predicting values for which no observations are available. The method is widely used in geostatic mapping and optimization studies, such as studies into optimal propeller designs. The Kriging approach basically works by taking a number of known points in the domain, evaluating the value of the function in those points and approximating the surface of the function using these values. Hence, this approximation surface or response surface is used to fill the domain. The method is a so-called spatially weighted prediction method. The following benefits can be identified:

- The estimates by Kriging are expected to be more accurate compared to traditional regression methods, especially for non-linear relationships [26].
- The Kriging model provides not only an estimate of the value at any specific point but also an indication of the prediction error and measurement uncertainty [9]. Since the uncertainty of the experiments is unknown, this could be very useful to quantify the confidence level of the prediction model.
- Flexibility of the model. The ability to simply and accurately accommodate a broad range of data sets [7].
- Kriging allows controlling the influence of data points on the estimation. Outliers can be ignored in creating the response surface [26].
- The algorithm contains an automated parameter estimation. This is in contrast with other regression methods, such as polynomial regression where the order has to be pre-defined. With Kriging, the chance of over-fitting of the data is therefore smaller.

Since the application of Kriging provides accurate predictions and has also proven itself in some studies in the field of propeller performance, it is decided to use the Kriging approach to build a model of the side force. In addition, an alternative approach is also used by means of a polynomial regression method. The purpose is to assess whether the side force can be represented by a polynomial function and to compare the Kriging approach with a less complex and more conventional regression method. The two approaches are briefly discussed below.

In the **first approach** the polynomial regression method is used. The polynomial function can either be given by a linear equation or higher order equation and be written as:

$$f(x) = w_0 + w_1 x + w_2 x^2 + ... + w_m x^k \tag{4.8}$$

The regression coefficients represent the independent contributions of each input variable to the prediction of the output variable. Its regression coefficients w are determined by estimation methods. The most common is the least-square estimation. The least square method minimizes the variances of the unbiased estimators of the coefficients. Equation 4.8 contains only one dependent variable. From the experimental results it is identified that the side force depends on two input variables, namely the advance and incidence angle. Equation 4.8 can also be expressed as function of the two input variables:

$$f(x) = w_0 + w_1 x_1 + w_2 x_2 + w_3 x_1^2 + ... + w_m x^k \tag{4.9}$$

The parameter k in equation 4.8 and 4.9 presents the order of the polynomial function. To choose the order of an approximate polynomial the forward selection procedure can be used [24]. The approach is

to successively fit the models in increasing order and test the significance of the regression coefficients at each step of model fitting. While there might be a temptation to fit a higher degree polynomial to get lower error, this can result in over-fitting. To prevent this, a different approach can be used in which the order is chosen by looking at the trend in the data. From figure 4.2, it is expected that a 3th order provide a good fit of the data.

In the **second approach**, the Kriging regression method is used. A detailed description of the mathematical algorithm can be found in [7] [9] [26]. The main idea is that processes varying across a space or time can be characterized by two major components. One deals with large-scale variations, typically a trend. The other one deals with small-scale variations and is typically relegated to the error term. The idea is that the prediction of $\hat{y}(x)$ for the known response $y(x)$ is realized in the Kriging approach with a regression model h(x) and a random function z(x), which can be written as:

$$\hat{y}(x) = h(x) + z(x) \tag{4.10}$$

In "universal Kriging", the regression model is a linear combination of k chosen polynomial regression functions. In our case a zeroth order polynomial (i.e. constant) is chosen, also so-called "Kriging mean". The random function z(x) is modelled with the process variance and a Gaussian process based correlation model. In theory, the Kriging approach is closely related to regression models. Although Kriging is an approach based on the assumption that an unknown point can be estimated by the weighted sum of some given samples at various location. As in other regression approaches, the relation between one sample point and the unknown point depends on the distance between those points. It is expected that the predictions by Kriging are more accurate. A practical guide into modelling of the Kriging regression method is presented in [7] and [9]. Similar as in the first approach, the input variables are the advance angle and incidence angle, and the output is the side force coefficient.

Stage 3: Performing the regression analysis and model testing
The procedure of creating the prediction model is split into three parts:

1. The regression coefficients are derived from the MARIN experimental measurement data.
2. Cross-validation is done to estimate the performance of the prediction model.
3. The new prediction model is validated by using the computed fit for data points of the other data sets and compare the outputs.

Cross-validation is a general technique for estimating the performance of a predictive model. It involves partitioning the data into data subsets and using one data set to predict the data left from the training set. A random set of data points is partitioned from the MARIN data set. The technique is often used in case not enough data sets are available for validation.

To evaluate the performance of the approximation model evaluation metrics are chosen. The main evaluation metrics used for regression are the root mean square, the mean absolute error and coefficient of determination. The **root mean square** was already presented.

The **mean absolute error** measures the average magnitude of the errors in a set of predictions. It is the average over the test sample of the absolute differences between prediction and actual observation where all individual differences have equal weight. The formula for MAE is shown in equation 4.11.

$$MAE = \frac{1}{n}\sum_{i=1}^{n}|y_i - \hat{y}_i| \tag{4.11}$$

The **coefficient of determination**, which is also known as R^2, is a standard way of measuring how well the model fits the data. It can be interpreted as the proportion of variability in a data set that can be explained by the statistical model. R^2 can take 0 as minimum, and 1 as maximum. Values close to 0 present a 'bad' fit and values close to 1 are 'good' fits. The formula for R^2 is

$$R^2 = 1 - \frac{\sum(y_i - \hat{y}_i)^2}{\sum(y_i - \bar{y}_i)^2}, \tag{4.12}$$

where $\bar{y}_i$ is the mean of the observed data.

4.3.3.2. Results regression analysis of side force coefficient

The regression analysis is performed by using the two approaches. Results are presented and discussed in this section.

Result polynomial regression

Figure 4.10 shows the fit between the MARIN measurement data and the predicted data. The evaluation metrics are included in the plot. A reasonable fit between the prediction model and the measurement data is found. This means that a 3th order polynomial is able to correctly predict the measurement data. To improve the performance of the prediction model, one could increase the order of the polynomial function. However, it is observed that this lead to over-fitting and an unrealistic trend.

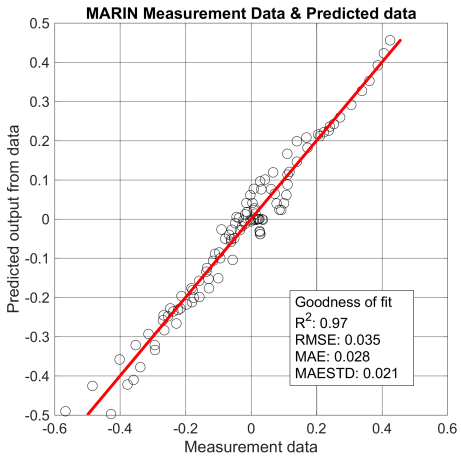

Figure 4.10: Predict output versus MARIN measurement data, result polynomial regression

In an attempt to validate the prediction model, the cross-validation technique is applied. A random set of data points is excluded from the training data set. The training set is used to derive a prediction function and validated with the excluded data set. The accuracy of the derived model is presented by the RMSE value. A value of 0.037 is found, which means that the error increased with 6%. This is an acceptable error level to validate the model.

In a second attempt to validate the prediction model, the polynomial function is used to predict the data observed in the RSD measurement. The results are displayed in figure 4.11. As one can see, a R^2 of 0.89 is found which indicates that the prediction model is able to predict 89% of the side force coefficient C_y correctly.

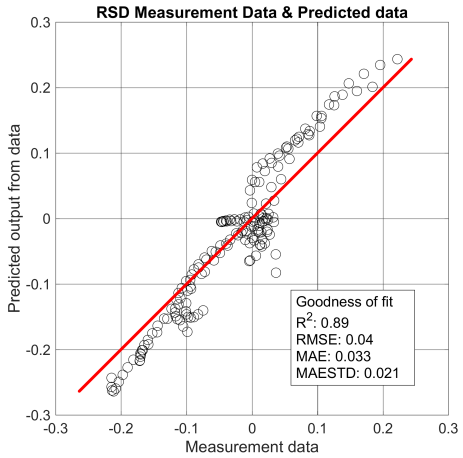

Figure 4.11: Predict output versus RSD measurement data

Results Kriging regression

The results of the Kriging regression analysis are displayed in figure 4.12. The predictions function is derived from the MARIN measurements data set. As one can see, an almost perfect fit is found with the measurements. Kriging approximated a measurement uncertainty of 1%.

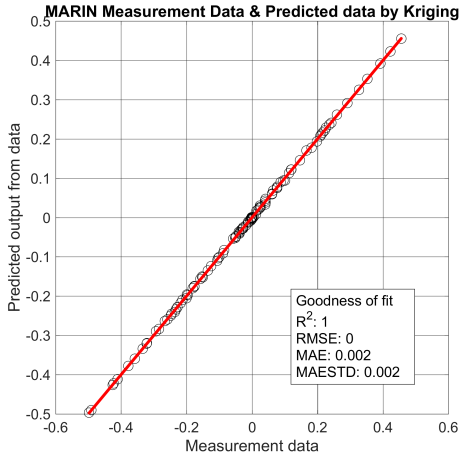

Figure 4.12: Predict output versus MARIN measurement data, result Kriging regression

To test the performance of the prediction model, 10% of the data is excluded and a cross validation analysis is performed. The prediction model was able to predict the side force coefficient C_y with a RMSE of 0.01. This is around 8% of the mean side force coefficient, which is acceptable to validate.

An alternative attempt to validate the prediction model by Kriging is to predict the RSD measurement data and determine its performance. Figure 4.13 presents the results and shows that the model is able to predict the measurement data with sufficient accuracy. The coefficient of determination R^2 indicates a value of 96%. The MAE increased with a factor of almost 10, but the error is still relatively low with respect to the absolute values.

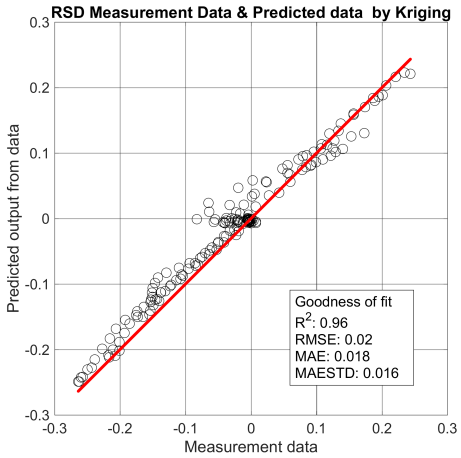

Figure 4.13: Predict output versus RSD measurement data

4.3.3.3. Conclusion regression analysis

Two approaches are used to derive an empirical model from measurement data. The results showed that the Kriging regression method performs better than the polynomial regression method. With a fit of 96% the model can adequately predict the side force coefficients measured in the RSD experiment. The polynomial function with a 3th degree order was also able to derive a fit of 89%, which is significantly lower with respect to the Kriging method. An attempt to improve the fit by increasing the order of the function didn't provide an improvement as unrealistic trends were found.

A benefit of the prediction function in form of a polynomial function is the simple mathematical representation in comparison to the prediction model by Kriging. Kriging provides a mathematical representation which is more like a black box and therefore the physical meaning is difficult to interpret. In general, the prediction algorithm requires more computational effort and time. The amount of data which is used to derive the model is however not large and didn't utilize significant computational time in comparison to the polynomial function.

It is concluded that the prediction model by Kriging mimics the behaviour as a function of the advance angle and incidence angle better in comparison to the polynomial model. Therefore, it is decided to use the prediction model derived with the Kriging regression method.

4.4. Results

(Not publicly available)

5

Two thrusters in open water

Nowadays tugs perform towing operations by multiple azimuth thrusters instead of a fixed propeller and rudder. The multiple propulsor configuration gives the flexibility to work faster and apply a higher towing force. Due to the fact that the thrusters are positioned relatively close to one another their performance is influenced. To investigate the interaction between the thrusters, the thruster performance of two thrusters in open water was measured. The measurements were done in the same angle thruster sweep test. During the sweep test both thrusters made a 0° to -180° rotation in azimuth. The tests are performed with the vessel sailing astern. It is assumed that this condition is close to open water conditions.

First, a validation study was performed to determine the performance of TUGSIM in the conditions where thrusters interact. The results are presented in the first section. Second, a theoretical model that calculates the impact of interacting thrusters on the thruster performances is proposed in section 5.3. Finally, the last section presents the comparison between the enhanced thruster performance model and the experimental data.

In this chapter, the port thruster is often called the leading or front thruster. The starboard thruster is denoted as the trailing thruster or rear thruster.

5.1. Validation study

(Not publicly available)

5.2. Investigation of two thrusters in open water

(Not publicly available)

5.3. Mathematical model

In the previous section it was shown that the interaction between the thruster can have a dramatic effect on the thruster performance. However, it is essentially confined to the trailing thruster for a combination of drift and thruster angle. Taking the interaction effect into account is considered to be essential to make a good prediction of the tug's performance. Brandner [3] developed an analytical model to predict the impact on the thruster performance. The objective of his study was to develop a simple model that is suitable to predict the relevant trend. Impact of the interaction effect is expressed by the flow properties (i.e. velocity and orientation) at the inlet of the trailing thruster. Based on the

inflow conditions, thrust and side force can be derived from the characteristics of a single thruster. Brandner found that the influence of interaction can be separated into three specific flow effects:

- Race impingement
- Race Wake
- Flow rectification

Race is defined here as the wake produced by the front thruster. Each effect is discussed in the sections below and mathematical relations are presented for their modelling. For a detailed explanation, see Brandner [3].

5.3.1. Race Impingement

Maximum interaction generally occurs where there is direct impingement of the wake. For a combination of drift and thruster angle, the high energy or exhaust part of induced flow from the leading thruster is directed towards the trailing thruster. The leading propeller derives its propulsive thrust by accelerating the fluid in which they work. The accelerating effect is enhanced by the nozzle fitted around the propeller. It is assumed that the thruster imparts an uniform acceleration to all the fluid passing through it. This induced accelerated water flow coming from the propeller is called the propeller race or wake. In certain conditions, the trailing thruster is working in water which is disturbed by the accelerating effect of the leading thruster. A change in the orientation and velocity of the flow is experienced by the thruster. To predict the thruster force, it is required to define the properties of the wake. The following properties of the race need to be determined:

- Mean velocity V_R of the race at duct exit from the leading thruster
- Trajectory of the race (i.e. orientation and cross section area affected by thruster wake)

To determine the mean velocity of the race, the linear momentum theory or so-called disk actuator theory is used. From basic momentum theory, we know that the amount of thrust depends on the mass flow rate through the propeller and the velocity change through the propulsion system. If the amount of thrust is known, the mass flow rate and velocity range can be determined. To determine these quantities, an appropriate control volume is defined enclosing the thruster and upstream part of the induced stream tube, as shown in figure 5.1. The stream tube entrance is located sufficiently upstream to assume free stream conditions and the exit is coincident with the duct exit.

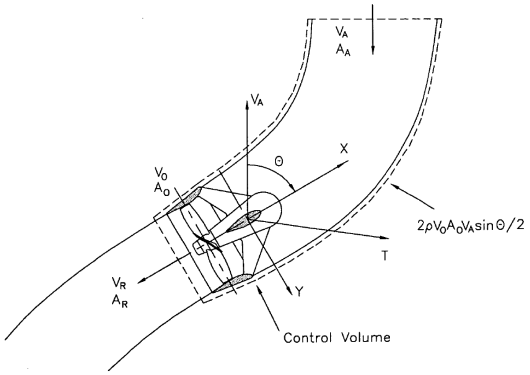

Figure 5.1: Geometry of thruster stream tube and control volume for calculation of initial race velocity

The linear momentum equation for applications of steady flow and where the control volume is fixed and rigid may be written as follows:

$$\oint_{A_{CV}} \rho \vec{V} (\vec{V}_{rel} \cdot \hat{n}) dA = \sum \vec{F} \tag{5.1}$$

The left side of the equation above is the momentum flux term. The change in momentum can be evaluated from the velocities at the entrance and exit of the stream tube as follows:

$$\oint_{A_{CV}} \rho \overrightarrow{V}(\overrightarrow{V}_{rel} \cdot \hat{n}) dA = \rho A_o V_0 (V_R - V_A \cos\theta) \tag{5.2}$$

Any effect of rotation which may be imparted to the fluid is neglected in the above expression. V_0 is the velocity close to the disc. The force term in equation 5.1 comprises the two external forces acting on the control volume, the thrust in longitudinal direction F_x and the net force inducing the curvature in the stream tube. The net force inducing curvature in the stream tube is assumed to be simply that required to deflect a streamline with velocity V_A through the incidence angle θ to velocity V_0. The two terms can be formulated as follows:

$$\sum \overrightarrow{F} = F_x - \rho A_o V_0 V_A (1 - \cos\theta) \tag{5.3}$$

Using the continuity equation for the mass per unit time through A_o to A_R, shows that the velocity at the disc V_o is equal to velocity at the exit V_R. The velocity V_o in the equations above may therefore be replaced with V_R. In applying the momentum theory to propeller race calculation, it is generally accepted that an empirical coefficient, the so called race coefficient k, is applied to calibrate the model and obtain the correct velocity of the race. The coefficient is commonly applied to the thrust term F_x. Combining equations 5.2 and 5.3 results in an expression which is rewritten to V_R:

$$V_R = \frac{1}{2}\left[V_A(2\cos\theta - 1) + \sqrt{V_A^2(2\cos\theta - 1) + \frac{4kF_x}{\rho A_o}} \right] \tag{5.4}$$

It is more convenient to consider the velocity of the race in terms of an advance velocity β_{PR}. The above equation is rewritten as follows:

$$\tan\beta_{PR} = \frac{1}{2}\left[\tan\beta_P(2\cos\theta - 1) + \sqrt{\tan^2\beta_P(2\cos\theta - 1) + \frac{4kC_x}{\cos^2\beta_P}} \right] \tag{5.5}$$

The race coefficient k is determined from the experimental results using the so-called thrust identity technique. This involves the comparison of the open water characteristics found in chapter 4 with those measured in open water conditions with thruster-thruster interaction. The objective of the method is to determine the mean advance angle β_P and incidence angle θ. The open water characteristics are defined by:

$$C_X = \frac{F_X}{\frac{1}{2}\rho A_o (V_A^2 + (0.7\pi n D_o)^2)} \tag{5.6}$$

$$C_Y = \frac{F_Y}{\frac{1}{2}\rho A_o (V_A^2 + (0.7\pi n D_o)^2)} \tag{5.7}$$

Rearrangement of the equation above in order to compare the measurements and the open water characteristics give the following two equations which need to be solved in order to determine the mean advance angle and angle of attack of the race.

$$C_X(\beta_P, \theta)(0.7\pi n D_o)^2) - \frac{X_{measured}}{\frac{1}{2}\rho A_o}\cos^2\beta_P = 0 \tag{5.8}$$

$$C_Y(\beta_P, \theta)(0.7\pi n D_o)^2) - \frac{Y_{measured}}{\frac{1}{2}\rho A_o}\cos^2\beta_P = 0 \tag{5.9}$$

The above equation is solved until:

$$\beta_P(X) - \beta_P(Y) = 0 \tag{5.10}$$

This procedure is done for a simple case of interaction between thrusters at an incidence angle of 0° in open water conditions and speed regime V_s = 0 Kn. By comparing the advance angle β_P determined with the thrust identity method and equation 5.5, the race coefficient k can be determined. A race coefficient of k = 0.7 is found. The specific physical meaning of the race coefficient is unclear. But

by evaluating the definition in equation 5.5 and its calculating procedure, it seems that the coefficient corrects the advance angle of the race to account for the spacing between the thrusters. Since the race of the leading thruster travels a distance of almost two diameters, it is expected that the race velocity changes compared to the velocity experienced at the outlet of the leading thruster. The change in race velocity is accounted for by the race coefficient k.

Having derived an expression for the race velocity at the inlet of the trailing thruster, it is possible to predict the trajectory of the race. This problem is closely related to that of a turbulent jet in a cross flow for which numerous experimental and theoretical studies are performed. The studies are discussed in more detail by Brandner [3]. Brandner used literature to develop a simple model that suitably predicts the relevant trends.

Similar to the derivation of the race velocity, the linear momentum theory is applied to derive an expression of the race trajectory. A global coordinate system aligned with the free stream for presenting the race trajectory is shown in figure 5.2.

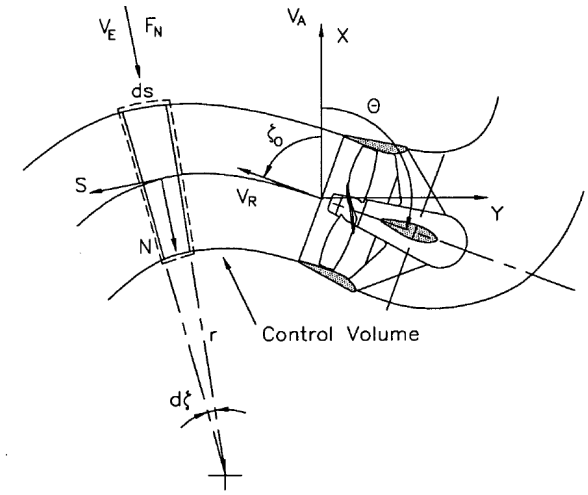

Figure 5.2: Global and local coordinate system for representing the race trajectory

The complete derivation of the momentum equation can be found in Brandner [3] and described in The Theory of Turbulent Jets by Abramovich [1]. The trajectory of a water particle coming from a thruster is defined by the cartesian coordinates

$$x_r = -\frac{\pi D_o \bar{x}_R}{2 C_N R_v^2}, \tag{5.11}$$

$$y_r = -\frac{\pi D_o \bar{y}_R}{2 C_N R_v^2}, \tag{5.12}$$

where an expression for $\bar{x}_R$ is derived from the momentum equation and defined as:

$$\bar{x}_R = \frac{e^{\bar{x}_R} \left| \tan \frac{\zeta_0}{2} \right|}{2} + \frac{1}{2 e^{\bar{x}_R} \left| \tan \frac{\zeta_0}{2} \right|} - \frac{1}{\sin \zeta_0} \tag{5.13}$$

ζ_0 is defined in figure 5.2 as the initial race angle at the outlet of the leading thruster with respect to the free stream. The velocity ratio R_V may be defined as:

$$R_V = \frac{\tan \beta_P}{\tan \beta_{PR}} \tag{5.14}$$

Equations 5.11 and 5.12 include the drag coefficient C_N. Abramovich [1] proposes that a typical value of 1.2 can be assumed for a turbulent jet in a cross flow. The race trajectory at a speed of zero knots is presented in figure 5.3.

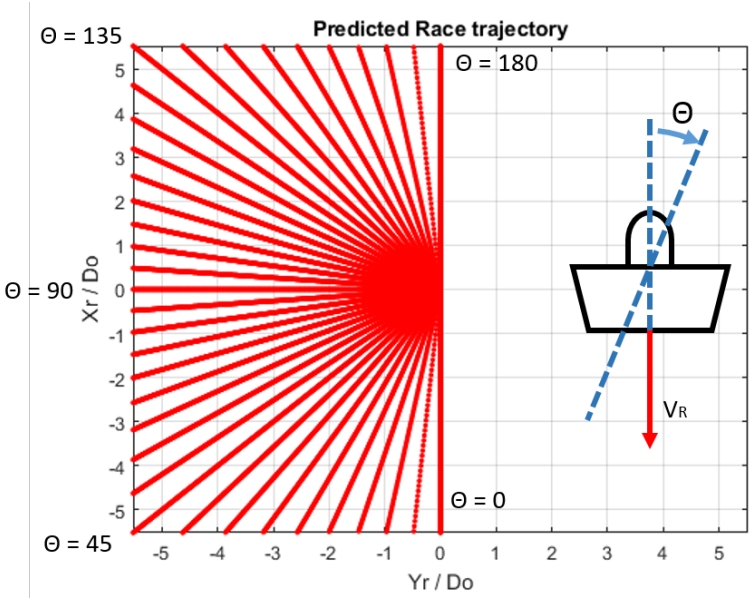

Figure 5.3: Predicted Race Trajectory for V_s = 0 and β_H = 0°

Having derived a method to determine the race trajectory, it is possible to determine the slope of the trajectory (i.e. the orientation of the flow with respect to trailing thruster). The slope of the trajectory can be derived by differentiating equation 5.13 at the location of the trailing thruster. The following equation is found:

$$\cot\zeta = \frac{d\bar{x}_R}{d\bar{y}_R} = \frac{e^{\bar{x}_R}\left|\tan\frac{\zeta_0}{2}\right|}{2} + \frac{1}{2e^{\bar{x}_R}\left|\tan\frac{\zeta_0}{2}\right|} \tag{5.15}$$

ζ represents the orientation of the inflow with respect to the free stream. Given the distance between thruster and race trajectory, it is possible to determine the proportion of the trailing thruster affected by the race of the leading thruster. This is determined by calculating the overlap of the thruster and the race cross section, as shown in figure 5.4. Using the principle of geometry, an expression is derived to determine the proportion of the thruster affected by the race:

$$\xi = \frac{1}{2\pi}\left[(\lambda_D - \sin\lambda_D) + \left(\frac{D_R}{D_D}\right)^2(\lambda_R - \sin\lambda_R)\right] \tag{5.16}$$

where,

$$\cos\frac{\lambda_D}{2} = \frac{4e^2 + D_D^2 - D_R^2}{4eD_D} \tag{5.17}$$

$$\cos\frac{\lambda_R}{2} = \frac{4e^2 + D_R^2 - D_D^2}{4eD_R} \tag{5.18}$$

ξ is the proportion of the thruster affected by the race and e is the minimum distance between the race and thruster, as shown in figure 5.4. For the present study, it is assumed that the race and thruster cross sections are of equal diameter. Larger cross sections could be assumed, however very little is known of the race cross section. Therefore it is decided to be conservative and assume similar cross sections. The minimum distance e is calculated by:

$$e = min\left(\sqrt{(x_{tl} - x_R)^2 + (y_{tl} - y_R)^2}\right) \tag{5.19}$$

x_{tl} and y_{tl} represent the relative location of the affected thruster. The location of the affected thruster is the center of the leading edge of the duct relative to the center of the trailing edge of the other, which

is considered more representative of the thruster's location. The following transformation in the free stream aligned coordinate system is derived to obtain

$$x_{tl} = s \sin \beta_H - L_{CLD} \cos \theta_{PS} + L_{CTD} \cos \theta_{SB}, \tag{5.20}$$

$$y_{tl} = -s \cos \beta_H - L_{CLD} \sin \theta_{PS} + L_{CTD} \sin \theta_{SB}, \tag{5.21}$$

where s, L_{CLD}, L_{CTD} are the thruster spacing, distance between centre of rotation and leading edge of duct and distance between center of rotation and trailing edge of duct respectively.

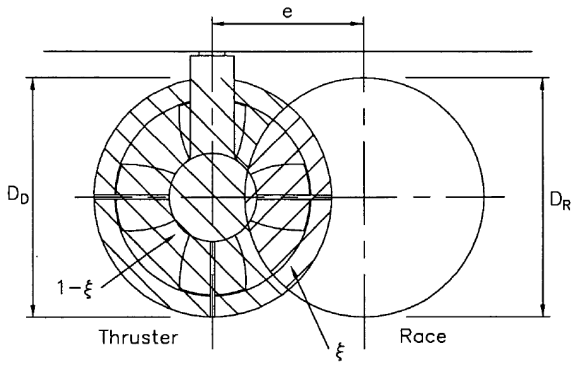

Figure 5.4: Overlap of thruster and race cross section

Based on the race advance angle β_{PR}, incidence angle θ_R and proportion of thruster affected ξ, thruster force can be calculated as follows:

$$F_X = \xi \cdot \Big(F_X(\beta_{PR}, \theta_R)_R - F_X(\beta_P, \theta_A)_A \Big) + F_X(\beta_P, \theta_A)_A \tag{5.22}$$

$$F_Y = \xi \cdot \Big(F_Y(\beta_{PR}, \theta_R)_R - F_Y(\beta_P, \theta_A)_A \Big) + F_Y(\beta_P, \theta_A)_A \tag{5.23}$$

So at maximum interaction, ξ is equal to 1 and subsequently gives a thruster force fully dominated by the force corresponding to an advance angle β_{PR} and incidence angle θ_R. As the thruster got less affected, ξ reduces up until zero and subsequently the thruster forces are fully defined by the free stream inflow properties β_P and θ_A.

5.3.2. Race wake effect

A complex flow phenomenon is observed by Brandner [3] when the race of a thruster is projected ahead of the affected thruster. Although free of direct impingement, thruster forces might still be affected by the race of the propeller. These effects are attributed to the wake region formed in the lee of the race. A sketch of the situation is presented in figure 5.5 to make it more clear. The lee of the race is indicated with the dotted red area. According to results by Brandner, it is shown that the advance angles approach zero, which means that the affected thruster is not subjected to the free stream anymore. In other words, the free stream flow field is blocked by the race and the inflow velocity approaches zero in these conditions.

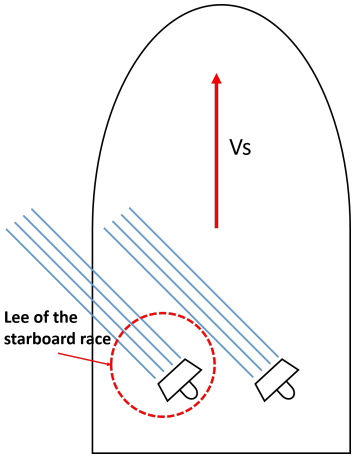

Figure 5.5: Sketch of race wake effect

Very little information describing the complex flow phenomenon is available. In absence of such information, it is assumed by Brandner that the wake is similar to that in the lee of cylinder. An identical cylinder is located in the wake of the upstream cylinder. Experiments of this configuration are conducted by Zdravkovich [28] and forces acting on the second cylinder are measured. These forces can be converted into a velocity and from the results a general trend is derived. From the data, it became clear that the distance between the cylinders define the velocity that is experienced by the second cylinder. This is included in a mathematical expression to determine the velocity in the wake of the race from an unaffected thruster. The expression is formulated as follows

$$\frac{V_{axr}}{V_A} = 1 - \left(1 - \frac{2\beta_H}{\pi}\right) e^{-0.015\left(\frac{x_R - x_{tl}}{D}\right)^{1.4}}, \tag{5.24}$$

where V_{axr} is the velocity in the lee of the race and experienced by the affected thruster. As can be seen in the equation, the effect of drift on the velocity is including the assumption that the wake varies linearly with the drift angle. The general trend is showed in figure 5.6. With increasing distance between the race and affect thruster, the velocity approaches free stream velocities. Finally, velocity V_{axr} is the input of the thrust force $F(\beta_P, \theta_A)_A$ in equation 5.22 and 5.23.

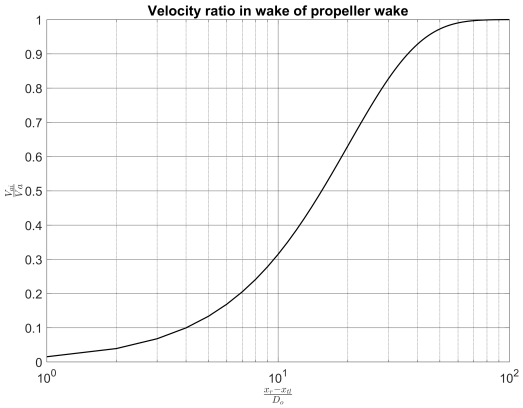

Figure 5.6: Velocity ratio as function of distance between wake and thruster

5.3.3. Flow rectification

As stated in section 5.2, thrust values do not return to the corresponding open water values despite being free from direct impingement of the propeller race of the leading thruster and its wake. The differences could be attributed to distortion of the flow field by the leading thruster. The leading thruster tends to bend the free stream in line with its longitudinal axis. As a consequence, the orientation of the

inflow of the trailing thruster is changed. This flow straightening effect created by the thruster is often termed as flow rectification. According to Brandner [3], this is mainly confined to large drift angles. As only zero drift angle is tested in the experiment, it is difficult to state whether this effect is also experienced in the experiments. Nevertheless, the effect is included in the mathematical model and is defined by the following equation:

$$\frac{\theta_t}{\theta_l} = 1 - 0.5\frac{2\beta_H}{\pi} \tag{5.25}$$

where t states for trailing thruster and l for leading thruster respectively.

5.4. Results

(Not publicly available)

6

Thruster in behind hull

The previous chapters discussed the thruster performance in open water. This chapter focuses on the thruster in behind hull. Along the thruster-thruster interaction, an interaction effect between hull and thruster is anticipated. Hull-thruster interaction is an important phenomenon for any ship, but for tugs it plays a particularly pronounced role due to the relatively large drift angles occurring during the operations and the flow around the hull and skeg [22]. Hull-thruster interaction can be separated into the effect of thruster on the hull and hull on the thruster. The latest effect is defined as the influence of the hull on the orientation and velocity of the flow at the location of each propeller. The interaction effect is reflected in the thruster forces. The effect of the thruster on the hull is not reflected in the thruster force. Since only the thruster forces and related interaction effects are investigated in this thesis, only the effect of the hull on the thruster is investigated.

To assess the impact of the hull on the thruster performance, the forces on the thruster units in open water are compared with thrusters in behind hull. By comparing the results of the two thruster experiments in open water, interaction effects between thrusters can be separated from those due to the hull. However, no experimental data of two thrusters in open water at drift is available. The two thrusters in open water tests are limited to zero drift angle. It isn't possible to use the data from the test at drift angle zero since the behaviour of thruster-thruster interaction effect varies with drift angle. Therefore to gain insight into hull-to-thruster interaction effect at drift, the prediction models from chapters 4 and 5 are used to generate the thruster characteristics in open water.

Since the prediction model is used to estimate the thruster performance in various conditions, this chapter indirectly describes the validation of the new prediction model for a thruster in behind hull.

The first section covers the validation of the current version of TUGSIM for the thruster in behind condition. Next, the results of the comparison between the predicted data and experimental data are presented. The focus of the investigation is three-fold; to study the effect of hull-thruster interaction, to test the validity of the new prediction model and to assess the impact of drift on the thruster performance.

6.1. Validation study

(Not publicly available)

6.2. Investigation of thruster in behind hull

(Not publicly available)

7

TUGSIM case study

In the previous chapters the new models are tested on a component level and are compared with model test measurements. It was concluded that the thruster forces can be predicted for various conditions with an acceptable prediction error. The proposed models are implemented in the original version of TUGSIM to determine the impact of side forces and thruster-thruster interaction effects on the escorting performance. Validation of the predicted escorting performance is not performed since no validation data is available of the RSD tug.

In this chapter, the implementation of the individual models in the TUGSIM environment is discussed. Followed by an assessment of the impact of the new models on the escort performance. Finally, conclusions are drawn and suggestions are proposed for the applicability of the new models in future version of TUGSIM.

Predictions are based on the RSD tug introduced in chapter 3. The escorting performance of the tug is estimated for a range of speeds and modes of operations. The range of speeds tested in the measurements with corresponding propeller revolution rates are studied. 10 knots is added to study the performance at high speed. Table 7.1 provides an overview of the operating conditions that are analyzed by TUGSIM.

Escorting mode	**Vessel speed V_s [kn]**
Indirect mode	0, 4, 8
Combination mode	0, 4, 8
Reverse/Transverse arrest mode	0, 4, 8, 10

Table 7.1: TUGSIM test cases

The escorting mode is characterized by its starting position with respect to the assisted vessel. This has mainly to do with the solving procedure in TUGSIM. To find all possible equilibria it is required to define various starting positions. The indirect mode starts at the bow of the assisted vessel. Combination and transverse arrest both start at the aft of the assisted vessel. Only in case of the transverse arrest, thruster steering angles are mirrored. All operation modes were highlighted in chapter 2.3.

7.1. Theoretical side force model

(Not publicly available)

7.2. Empirical side force model

(Not publicly available)

7.3. Thruster-thruster interaction model

(Not publicly available)

8

Conclusions and recommendations

An concise overview of the conclusions is presented in section 8.1. The limitations and recommendations for future work are covered in section 8.2.

8.1. Conclusions

In the introduction of this thesis the objective of this thesis is formulated:

The goal of this thesis is to quantify and increase the understanding of the azimuthing thruster forces and hydrodynamic interaction effects of a tug in escorting conditions in order to enhance the reliability of the TUGSIM calculation.

An opportunity was provided to conduct the research based on experimental data and achieve the research goal. The research project is broken down into validation, investigation and quantification. These aspects form the outline of the presentation of the conclusions. Finally, the conclusions related to the applicability in the TUGSIM environment and the impact of the new models on escorting performance prediction are presented.

8.1.1. Validation of original version of TUGSIM

A validation study of the propulsion model in TUGSIM was conducted to determine its reliability and identify missing phenomena related to propulsive forces. The following is concluded:

- (Not publicly available)

8.1.2. Investigation of the underlying physics

The introduction of this thesis highlighted three regions of interest that haven't yet been thoroughly investigated. Validation study confirmed that these regions are not yet well understood and consequently not fully captured by TUGSIM. A better understanding is gained of the regions of interest to a certain extent, considering the practical limitations of interpreting experimental data. From the investigation the following is concluded:

- The main driving component of the thruster forces in oblique flow is the nozzle. It can be explained by its operational principle.

- The contribution by the propeller to the total side force is small due to the flow straightening effect of the nozzle on both the propeller in and outflow. Therefore the propeller side force can be ignored.

- The effects of interaction between thrusters is essentially confined to the (trailing) thruster which is affected by the propeller race of the other (leading) thruster. The nature of interaction between thrusters exhibits variations with drift angle and speed.
- Thruster-thruster interaction is not only confined to direct impingement of the propeller race. When the trailing thruster is operating behind the propeller race of the leading thruster, inflow properties tend to deviate from the free stream values. However, the underlying physics are not well understood in this thesis nor in literature.
- The thruster that is free of thruster-thruster interaction effects encounters little influence of the presence of the hull. It can be satisfactorily represented as a single thruster in open water.
- The influence of the hull on the thruster, which is in the meantime subjected to thruster-thruster interaction effects, couldn't be identified. The interaction effect between thrusters couldn't be separated from the those from the hull.

8.1.3. Quantification

The goal was to develop quasi-steady prediction models that are able to predict the relevant trends. Based on the prediction results, the following is concluded:

- The theoretical side force model proved to be able to predict the overall trend of the side force .
- The empirical regression method based on experimental data was able to predict the side forces with a high accuracy. The Kriging regression method mimics the behavior of the side forces better in comparison to the polynomial regression method. In addition, Kriging is a very effective and quick method to generate an empirical relation from measurement data.
- The mathematical model for interaction between thrusters reasonably predicts the trend. Discrepancies can be attributed to prediction of the race trajectory. In addition, capturing the physics of the flow in the wake of the propeller race with the model was not possible. These physics are not well understood yet, mainly due to absence of information.

8.1.4. TUGSIM case study

From the preceding study more confidence is gained into the prediction of the thruster forces in escorting conditions. This flows into enhanced reliability of the TUGSIM calculation. Based on various simulation cases, conclusions are drawn on the applicability of the models and impact on the escorting performance. The following is concluded:

- (Not publicly available)

8.2. Limitations and recommendations

This section provides a discussion of the limitations of the study. Suggestions to overcome these limitations are formulated as research opportunities for future work.

(Not publicly available)

Bibliography

[1] Abramovich, G. (1963). The theory of turbulent jets. M.I.T. Press.

[2] Berchiche, N. and Krasilnikov, V. (2018). Numerical analysis of azimuth propulsor performance in seaways: Influence of oblique inflow and free surface. Journal of Marine Science and Engineering, 37(6):1–24.

[3] Brandner, P. (1995). Performance and Effectiveness of Omni-Directional Stern Drive Tugs. PhD thesis, University of Tasmania.

[4] Bulten, N. and Suijkerbuijk, R. (2013). Full scale thruster performance and load determination based on numerical simulations. International Symposium on Marine Propulsors, (3):501–509.

[5] Carlton, J. (2012). Marine Propellers and Propulsion. Butterworth-Heinemann.

[6] Dalheim, O. (2015). Development of a Simulation Model for Propeller Performance. PhD thesis, Norwegian University of Science and Technology.

[7] de Baar, J., Dwight, R., and Bijl, H. (2013). Improvement to gradient-enhanced kriging using a bayesian interpretation. International Journal of Uncertainty Quantification, 4:205–223.

[8] Fleming, J., Jones, T., Ng, W., Gelhausen, P., and Enns, D. (2003). Improving control system effectiveness for ducted fan vtol uavs operating in crosswinds. In 2nd AIAA" Unmanned Unlimited" Conf. and Workshop & Exhibit, page 6514.

[9] Forrester, A., Keane, A., et al. (2008). Engineering design via surrogate modelling: a practical guide. John Wiley & Sons.

[10] Gandin, L. S. (1965). Objective analysis of meteorological fields: Gidrometeorologicheskoe Izdatel'stvo (GIMIZ), Leningrad. Translated by Israel Program for Scientific Translations, Jerusalem.

[11] Gutsche, F. (1964). The study of ships' propellers in oblique flow. Defence Research Information Centre London.

[12] Hallmann, R. (2016). Reverse stern drive tug (24.6m); captive manoeuvring model tests, final report. MARIN.

[13] Johnson, E. and Turbe, M. (2006). Modeling, control, and flight testing of a small ducted-fan aircraft. Journal of Guidance, Control and Dynamics, 29(4):209–218.

[14] Jukola, H. and Castleman, G. E. (1995). Z-drive escort tug operating modes. Marine Technology.

[15] Klein Woud, H. and Stapersma, D. (2008). Design of propulsion and electric power generation systems. IMarEst.

[16] Matheron, G. (1963). Principles of geostatistics. Economic Geology, 58:1246–1266.

[17] Minaas, K. and Lehn, E. (1978). Hydrodynamic characteristics of rotatable thrusters. NFSI report R-69.78.

[18] Nienhuis, U. (1992). Analysis of Thruster Effectivity for Dynamic Positioning and Low Speed Manoevring. PhD thesis, Technical University of Delft.

[19] Oosterveld, M. (1973). Ducted propeller characteristics. The royal Institution of Naval Architects.

[20] Pavlioglou, S. (2015). A numerical investigation of a ducted azimuthing thruster in oblique flow. Master's thesis, Delft University of Technology.

[21] Pflimlin, J., Binietti, P., Soueres, P., Hamel, T., and Trouchet, D. (2010). Modeling and attitude control analysis of a ducted-fan micro aerial vehicle. Control Engineering Practice, 18:209–218.

[22] Quadvlieg, F. and Kaul, S. (2006). Development of a calculation program for escort forces of stern drive tug boats.

[23] Schulten, P. (2005). The interaction between diesel engines, ship and propellers during manoevring. PhD thesis, Technical University of Delft.

[24] Shalabh (1965). Regression Analysis. IIT Kanpur.

[25] Timmers, R. (1992). Sleep presetaties. 4e jaars scriptie, Damen Shipyards Gorinchem.

[26] Vesting, F. and Bensow, R. (2014). On surrogate methods in propeller optimisation. Ocean Engineering, 88:214–227.

[27] White, F. (1999). Fluid mechanics. MacGraw-Hill.

[28] Zdravkovich, M. (1973). Review of flow interference between two circular cylinders in various arrangements. Journal of Fluids Engineering.

[29] Zhang, Q., Jaiman, R., Ma, P., and Liu, J. (2018). Investigation on the performance of a ducted propeller in oblique flow.